EXPERIMENTS ON SMELT SHATTERING AND DISSOLUTION

MARKUS BUSSMANN, ERIC JIN, MICHAEL LIN, ANDREW JONES, HONGHI TRAN*

ABSTRACT

An effective and safe dissolving tank is key to proper management of a Kraft recovery operation. This paper presents results of two ongoing studies related to the dissolving tank. 1) A scaled-down experimental apparatus using water and air was used to examine shattering as a function of gas and liquid flow rates and of various gas nozzle geometries and positions. The objective was to identify best practices for smelt shattering. 2) A separate study involved visualizing the interaction of molten smelt droplets falling into water as a function of various parameters. Results to date demonstrate that droplets "explode" either at the water surface or beneath it as long as the water temperature is below a critical value. These droplet explosions, although violent, enhance smelt dissolution. However, as the water temperature rises, the explosions become less likely, and beyond a certain temperature, droplets do not explode at all, leaving solid smelt to accumulate on the tank bottom.

INTRODUCTION

Combustion of concentrated black liquor in the recovery boiler results in formation of molten smelt at the bottom of the boiler (Fig. 1(a)). Smelt consists mostly of Na_2CO_3 and Na_2S, with small amounts of Na_2SO_4, NaCl, and potassium salts [1]. Molten smelt pours out of the boiler at about 800°C (+/- 30° or so) through one or more smelt spouts. It is shattered by a high-pressure steam jet into small droplets (Fig. 1(b)) before falling into the dissolving tank, where it interacts with water and dissolves. The solution (green liquor) is causticized with lime in the causticizing plant to covert Na_2CO_3 into NaOH. The resulting solution, which contains mainly NaOH and Na_2S, is reused in the pulping process.

Although shattering molten smelt with a high-pressure steam jet and dissolving the shattered smelt in the dissolving tank are violent and often dangerous processes, they are necessary to process the large amount of molten smelt effectively and to produce consistent green liquor. Dissolving tanks constantly rumble and at times cause tremors of the ground and buildings nearby. The violent smelt-water interaction can also emit a cloud of water vapor/mist that contains malodorous and toxic reduced sulphur gases around the dissolving tank area, which at times can trigger evacuation. In severe cases, explosions can occur, causing substantial equipment damage and production loss associated with unscheduled boiler downtime. Personnel injuries and fatalities have also reportedly been caused by a tank explosion or by being showered with hot smelt and green liquor ejected from the dissolving tank. Over the past 30 years, approximately one explosion incident per year has been reported in North America [2], although the actual number could be higher because many incidents go unreported. Needless to say, one explosion incident is too many when it comes to workplace safety. As regulations on occupational health and safety have become increasingly stringent in recent years, effective and safe dissolving tank operation has become a top priority for Kraft pulp mills.

MARKUS BUSSMANN
University of Toronto
Toronto, On,
Canada
*Contact: bussmann@mie.utoronto.ca

ERIC JIN
University of Toronto
Toronto, On,
Canada

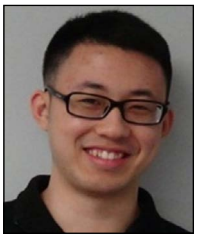

MICHAEL LIN
University of Toronto
Toronto, On,
Canada

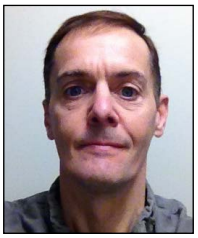

ANDREW JONES
University of Toronto
Toronto, On,
Canada

HONGHI TRAN
University of Toronto
Toronto, On,
Canada

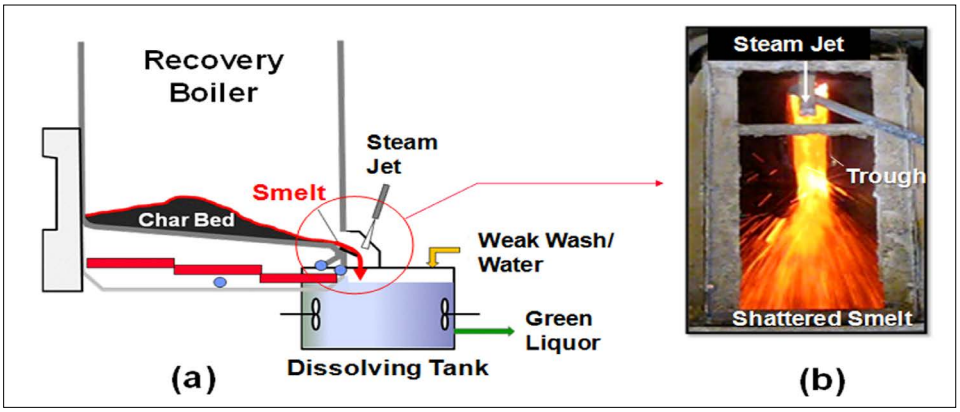

Fig. 1 - (a) Molten smelt stream from a recovery boiler; (b) smelt shattered by a steam jet.

Despite the importance of these problems, the triggering mechanism of a dissolving tank explosion, and the factors affecting an explosion, are not well understood. Shick and Grace [3] conducted a comprehensive literature review on liquid-liquid explosions in the early 1980s and suggested that smelt-water explosions involve the same vapour explosion mechanism as other liquid-liquid systems, where the high heat from one liquid causes the other liquid to vaporize rapidly. However, the interaction between smelt and water in the dissolving tank differs from other liquid-liquid systems in that one liquid (molten smelt) is highly soluble in the other (water). The composition and the amount of smelt dissolved are expected to have an effect on green liquor properties, and hence on dissolving tank explosions. Although liquid-liquid explosions have been intensively studied in the nuclear, metal processing, and liquefied natural gas industries [3–9], as well as in the field of oceanic volcano science [10], only two studies of smelt-water interaction in the dissolving tank environment have been published, both in the mid-1950s [11,12]. These studies were crudely carried out, and the results obtained were insufficient to draw quantitative conclusions.

This paper presents an overview of two ongoing studies being conducted at the University of Toronto on smelt shattering and dissolution. In each case, details of the methodology and of recent results are presented, as well as an outlook towards future work. These studies are being conducted as parts of a larger research program focussed on dissolving tank safety, which includes the development of a model of dissolving tank operation that will use the results of both studies.

THE STUDY OF SMELT SHATTERING

The study of smelt shattering was begun by Taranenko [13,14], who built an apparatus (Fig. 2) using an air jet to examine the shattering characteristics of water/glycerine mixtures as a function of air velocity, liquid viscosity, liquid flow rate, and air nozzle proximity. Water is pumped from the base tank to the inclined tank and subsequently flows down a spout at a prescribed rate. An air jet nozzle is positioned above the lip of the spout to shatter the exiting water stream. Both the air and water flow rates are controlled using valves and flow meters. An optical direct-imaging technique using a high-speed camera captures droplet size information.

Experiments were performed using a 7.9-mm (5/16") orifice full cone converging/diverging nozzle. The results were as expected: increasing the air velocity, decreasing the liquid flow rate, and reducing the distance between the nozzle and the water stream all reduce average droplet size, as shown in Figs. 3 and 4. The effect of liquid viscosity (1 to 50 cP) was also studied: mean droplet size increased with viscosity, as expected. The effect of liquid viscosity was most pronounced when shattering with a weaker jet (100 m/s at the nozzle exit). In that case, the mean diameter varied from 1.2 mm for the 1 cP liquid to 2.1 mm for the 50 cP liquid. At higher air velocities, droplet size varied less.

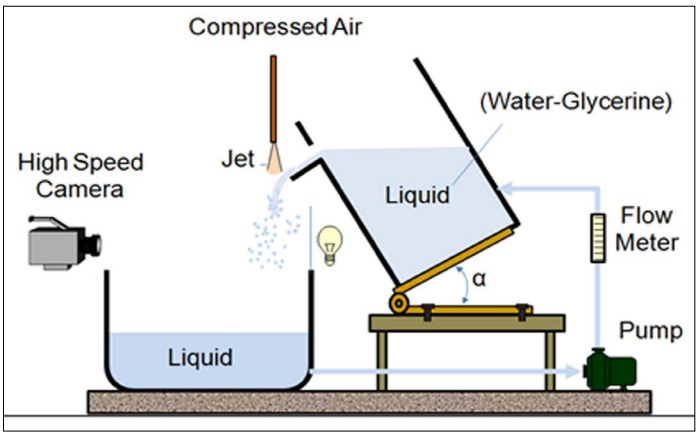

Fig. 2 - Laboratory-scale shattering apparatus.

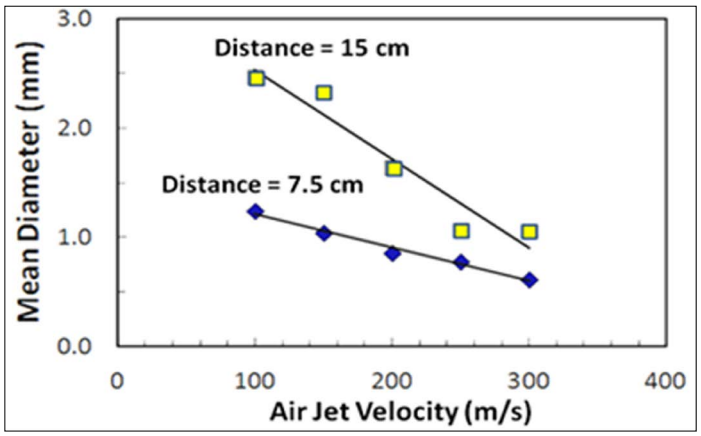

Fig. 3 - Effect of air jet velocity and nozzle distance from the liquid stream on the Sauter Mean Diameter (SMD) of the shattered liquid (liquid flow rate 0.1 L/s, viscosity 2.5 cP).

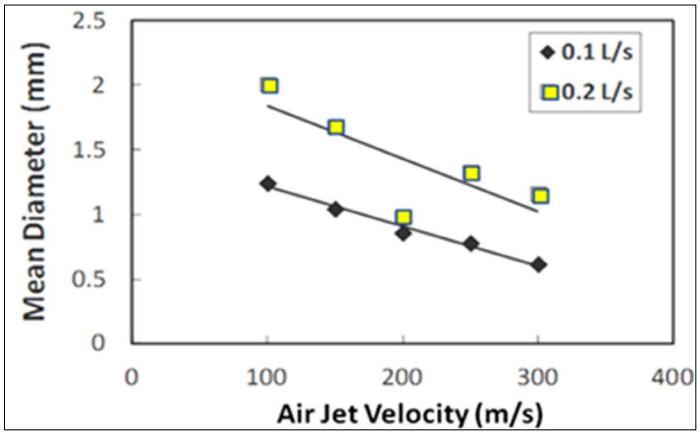

Fig. 4 - Effect of air velocity and liquid flow rate on SMD (liquid viscosity 2.5 cP, nozzle 7.5 cm from the liquid).

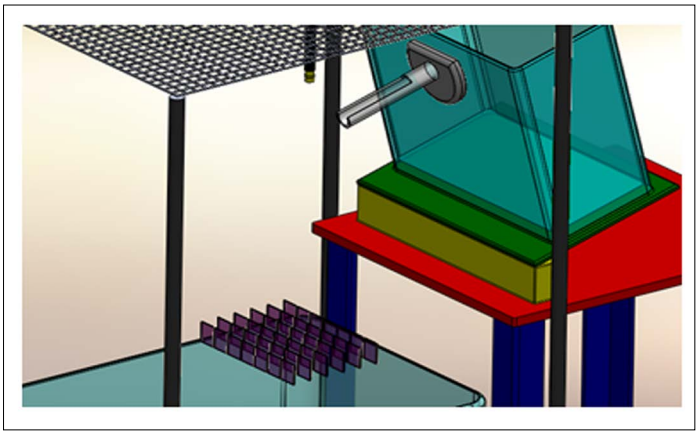

Fig. 5 - Schematic of the experimental set-up showing the array of 42 imaging locations.

Current Experimental Methodology

Recent improvements have focussed on characterizing the droplet size distribution across the spray and on automating the image analysis and processing functions. A matrix of locations is now imaged to capture a spatial distribution of droplets, and the ImageJ™ image analysis software is used to process the images and calculate the projected area of the droplets. This information is then used to calculate drop diameters [15]. The current study considers the effect of different air nozzles on shattering effectiveness.

As illustrated in Fig. 5, a 30 x 35 cm area 60 cm below the spout is imaged using a Mega-Speed™ greyscale high-speed camera. Images are recorded at 42 (6 x 7) evenly spaced locations. The camera records 50 frames per second for 10 s at each location; the exposure time is 50 □ s, the focal length 200 mm, and the f-stop 3.5. A light source with a diffuser is placed behind the liquid stream to provide sufficient lighting. The camera captures and stores grayscale images at 512 x 512 resolution. Only water was used for these latest experiments, at a flow rate of 0.2 L/s. A grid system mounted above the apparatus is used to focus the camera at each imaging location.

Using the ImageJ software, an image analysis macro was developed to convert each grayscale image into a binary image and to filter out-of-focus droplets that cannot be accurately measured (Fig. 6). The images are dimensionally calibrated, and the program measures the projected area of the droplets. Droplets cut off at the edges of the frame are not measured. Due to the resolution of the camera (512 x 512 pixels), it is difficult to determine whether very small droplets are in focus because they cover only a few pixels. These droplets are discounted to prevent skewing of data; therefore, only droplets of greater than 0.16 mm diameter are counted and analyzed. The average droplet projected area and count is calculated from 500 images at each of the 42 locations. Tecplot™ software is then used to plot the average droplet diameter and the droplet count distribution for each experiment, as shown in Fig. 7.

Four different laboratory-scale nozzles were tested at various nozzle distances, orientations to the liquid stream, and gas flow rates. The nozzle profiles are representative of nozzles in use by industry.

TABLE 1 *Experimental parameters.*

Nozzle orientation (from horizontal)	90° (vertical), 75°, 60°
Proximity to impingement	23, 18, 13 cm (9, 7, 5 in)
Air flow rate	283, 354, 425 L/min (10, 12.5, 15 SCFM)

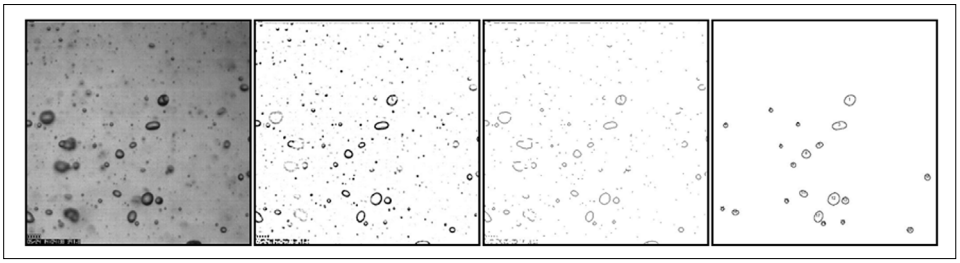

Fig. 6 - The series of imaging processes used to filter out-of-focus droplets.

The top part of Fig. 8 illustrates the four nozzles. Table 1 lists the range of each parameter.

Preliminary Results and Discussion

Figure 8 illustrates the preliminary droplet size and droplet count distributions for each of the four nozzles at two air flow

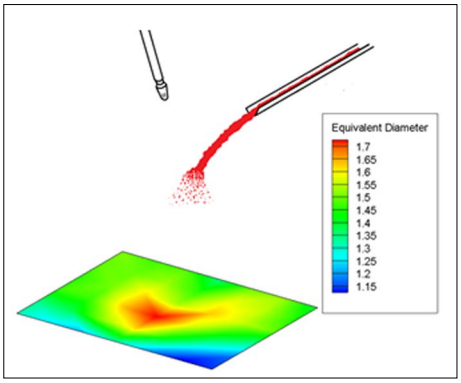

Fig. 7 - A sample contour illustrating average drop diameter (mm).

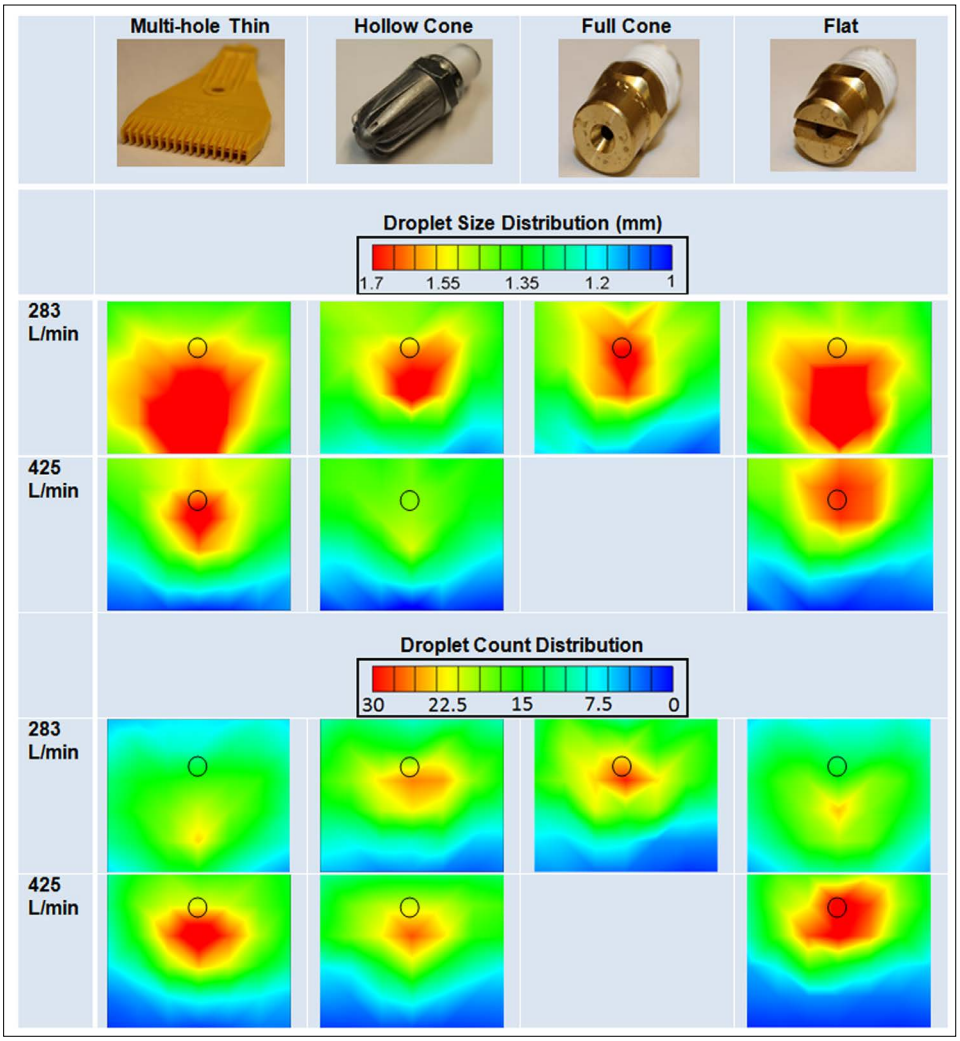

Fig. 8 - Droplet size and droplet count distributions over the 30 x 35 cm area 60 cm below the spout. The black circle represents the air nozzle location. The top of each contour is nearest the spout.

rates, corresponding to the experimental set-up illustrated in Figs. 5 and 7. These experiments were conducted with the nozzle at a 90° (vertical) orientation, 18 cm above the point of impingement. The spout was tilted at 15°.

The results clearly show that different nozzles produce different droplet size and count distributions. At 283 L/min, the multi-hole thin nozzle and the flat nozzle produce generally larger droplets across a larger area than the hollow cone nozzle or the full cone nozzle. When the air jet impinges the water stream, the droplet trajectory is determined by the transfer of kinetic energy from air to water. Atomization occurs by continually shearing layers of the water stream. The top layer of the water stream receives the greatest amount of kinetic energy from the air and hence is atomized more effectively, resulting in smaller droplets with higher kinetic energy scattered across a wider area. The underside of the liquid stream receives less kinetic energy from the air jet, resulting in larger droplets that retain more of their initial momentum. Both the multi-hole thin nozzle and the flat nozzle produce less shattering, so that the largest droplets (in the red zone) are further from the nozzle. This is due to the wider air distribution that these nozzles produce, which reduces the amount of air that actually impacts the water stream. The hollow cone and full cone nozzles produce smaller droplets in general, and the centre of the red zone is closer to the nozzle.

Increasing the air flow rate to 425 L/min leads to a significant reduction in droplet size. For the multi-hole thin and flat nozzles, the largest droplets are closer to the nozzle, indicating a higher kinetic energy transfer from air to water. It was impossible to run the full cone nozzle experiments at an air flow rate of 425 L/min because the nozzle could not be kept attached to the air supply line.

The droplet count distributions at 283 L/min show that the hollow and full cone nozzles produce a greater number of droplets near the nozzle and few further from the spout. The highest droplet count is concentrated near the area with the greatest droplet diameter. When the flow rate increases to 425 L/min, the droplet count increases significantly because the higher air flow rate shatters more effectively, producing smaller droplets and more of them.

THE STUDY OF SMELT/WATER INTERACTION

Work by the authors to date on smelt/water interaction [16,17] has focussed on the effects of smelt temperature and water temperature on the behaviour of droplets falling into water. This section will review some of those results and provide a look ahead to future research.

Experimental Setup

The synthetic smelt used in this study was a mixture of 80wt% Na_2CO_3 and 20wt% NaCl powder. This composition was chosen because the sample has a complete melting temperature of 750°C, meaning that it would be completely molten in the crucible at the temperatures examined. A schematic of the experimental apparatus used in the study of smelt-water interaction is shown in Fig. 9.

A 220 mm-long cast alumina (Al_2O_3) tube crucible with a 30-mm ID open top end and a 3-mm ID hole at the tapered bottom end is housed in a tubular electric furnace. A cast Al_2O_3 rod is inserted vertically into the crucible from the top to seal the hole loosely at the tapered bottom end.

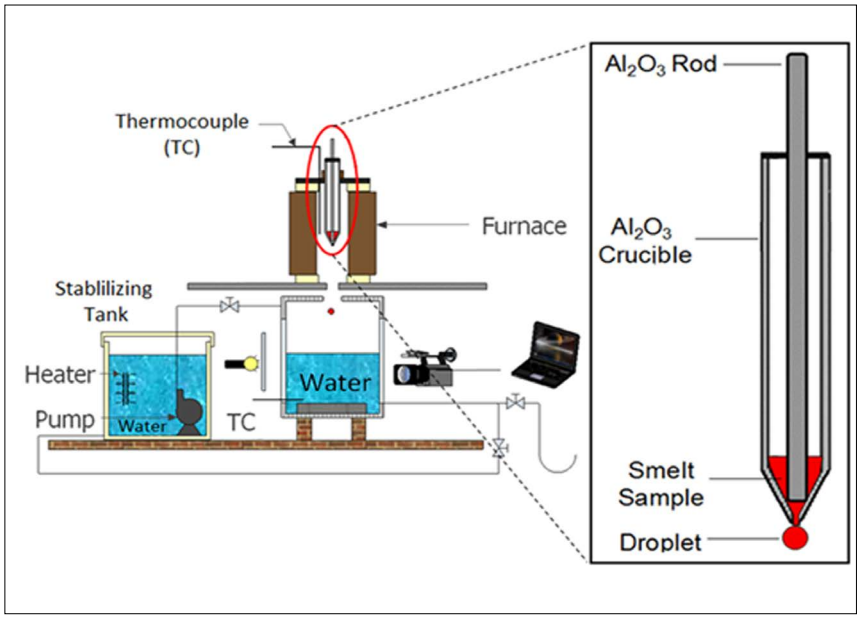

Fig. 9 - **Experimental apparatus for the smelt-water interaction experiments.**

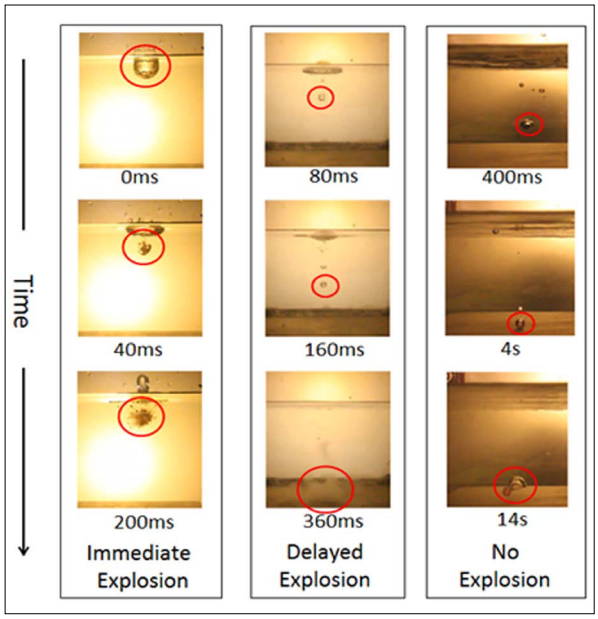

Fig. 10 - **Three smelt-water interaction regimes (the red circles highlight the droplets).**

Pulverized synthetic smelt is fed into the crucible from the top and accumulates at the bottom, in the space between the crucible and the rod. As the crucible is heated in the furnace to the desired temperature, molten smelt begins to seep out from the crucible through the rod seal, and a droplet eventually falls out of the crucible from the bottom hole.

A 22-litre rectangular main tank is located beneath the furnace. It consists of stainless steel side walls and transparent polycarbonate front and back walls so that the behaviour of smelt droplets can be observed. Water is heated in a 40-litre stabilizing tank using a temperature-controlled coil heater and circulated between the two tanks through a submersible pump. A video camera with a frame rate of 25 frames per second is placed in front of the tank to record the behaviour of each smelt droplet as it falls into the tank and interacts with water. Two light bulbs and a diffuser are mounted behind the back wall of the tank to illuminate the experiment. A computer connected to the video camera enables real-time monitoring of smelt-water interactions in the water tank and storage of video data.

In this study, the size of the droplets was approximately 7 mm, as measured by comparing video images with a calibrated image. The droplets fell about 700 mm, and the water level in the tank was 120 mm. Experiments were carried out at three smelt temperatures (T_s): 800°C, 900°C, and 1000°C, and the water temperature (T_w) was varied between 25°C and 100°C. For each condition, at least 30 droplets were generated.

RESULTS AND DISCUSSION

The behaviour of a molten smelt droplet in water was studied as a function of smelt temperature and water temperature, keeping other variables such as smelt composition constant. The series of photos recorded by the video camera show three distinct interactions, which are illustrated in Fig. 10. Some droplets break into small pieces upon contact with water and disintegrate immediately at the water surface (*immediate explosion*). Some sink beneath the water surface and explode either in the middle of the water tank or after settling on the tank floor (*delayed explosion*). Finally, some droplets sink to the bottom of the tank and solidify without exploding (no explosion). To quantify the effects of T_s and T_w on the interaction, the "explosion probability" and "explosion delay time" (*dl*) were investigated.

The probability of explosion was calculated by dividing the number of droplets that exploded by the total number of droplets tested for each experimental condition (approximately 30). As shown in Fig. 11, at a given T_s, there is a water temperature range below which the explosion probability is 100% (i.e., droplets always explode) and above which the explosion probability is 0% (i.e., no droplets explode). The low end of this temperature range defines the lower critical water temperature, *Lower* $T_{crit,w}$, and the high end defines the upper critical water temperature, *Upper* $T_{crit,w}$. The results clearly show that *Lower* $T_{crit,w}$ decreases with increasing smelt temperature: 72°C for Ts= 800°C, 65°C for Ts= 900°C, and 50°C for T_s=1000°C. *Upper* $T_{crit,w}$, on the other hand, remains the same at 82°C for all cases. The explosion probability for a real Kraft smelt sample at 800°C was also tested and was found to follow the same pattern as the synthetic smelt. However, not too much should be read into this result because subsequent experiments (yet to be published) on the effect of smelt composition, which was investigated by varying the ratio of Na_2CO_3 to NaCl, have shown that composition can have

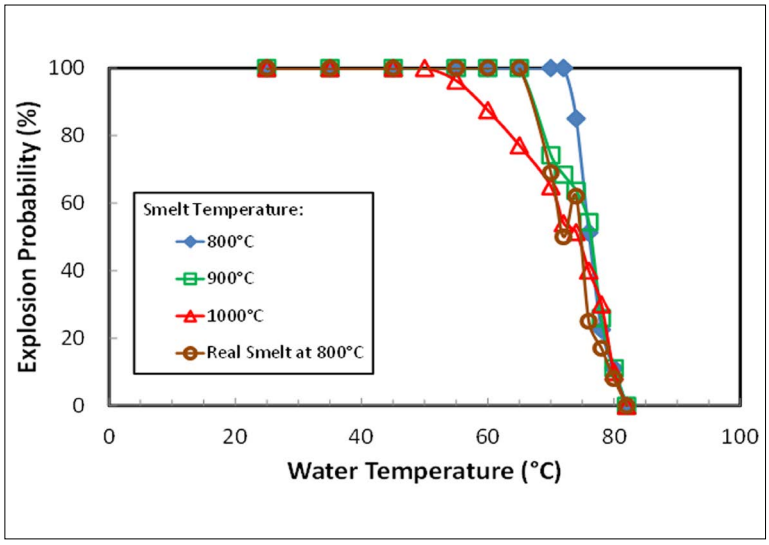

Fig. 11 - Explosion probability at different water (T_w) and smelt (T_s) temperatures.

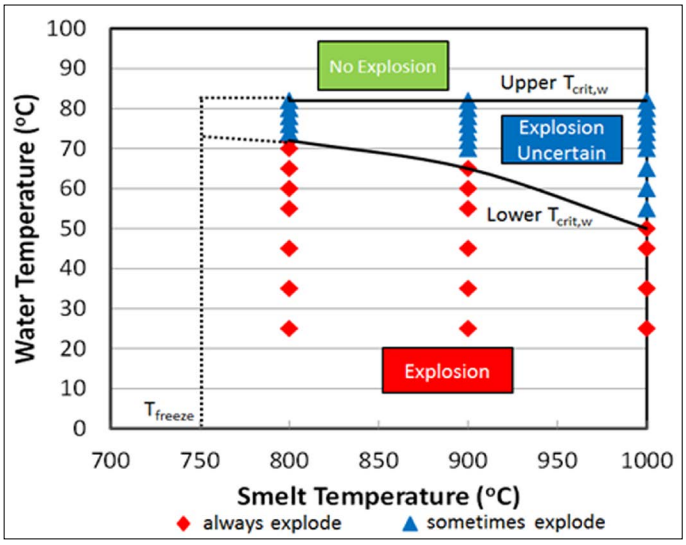

Fig. 12 - Smelt-water interaction temperature (SWIT) diagram (80% Na_2CO_3 and 20% NaCl).

a significant effect on smelt-water interaction.

The data in Fig. 11 can be considered to show the combined effect of T_s and T_w on the explosion probability of molten synthetic smelt droplets; this will be referred to as a *smelt-water interaction temperature* (SWIT) diagram, as illustrated in Fig. 12. The diagram predicts how molten smelt and water will interact at different temperatures. Below the *Lower* $T_{crit,w}$ curve, droplets always explode. Above the *Upper* $T_{crit,w}$ line at 82°C, no droplets explode. Between the lower and upper critical water temperatures, a droplet may or may not explode. The left boundary of the SWIT diagram is the freezing temperature of the synthetic smelt, 750°C, although droplets may explode at lower temperatures if supercooled or only partially frozen.

The explosion delay time (*dt*) is defined as the duration between first contact with water and when a droplet explodes. The contact time was determined from the video recordings, and the explosion time was obtained from the acoustic signal recorded by the camera. Figure 13 illustrates the droplet explosion delay time at different smelt and water temperatures. At a given T_s, dt increases with increasing T_w; *dt* also increases as T_s increases.

The explosion delay time offers insight into the effect of the tank bottom on droplet behaviour. With 120 mm of water in the tank, droplets take about 0.4 s to impact the tank bottom for the first time; if they bounce and do not explode, the second impact usually occurs at *dt*=0.8 s. Figure 14 superimposes the data of Figs. 11 and 13 to illustrate explosion probability and delay time at different T_w. Note that the delay-time curves plateau at about 0.4 s for all three smelt temperatures and that towards the end of each plateau, the corresponding explosion probability begins to decrease. This suggests that impact on the tank bottom can trigger some droplet explosions and that only an incremental rise in T_w can overcome the effect of the tank bottom, so that dt begins to rise again. The droplets that survive the first

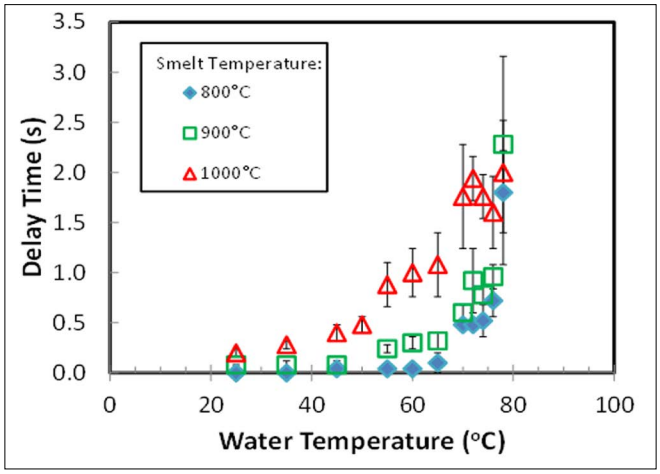

Fig. 13 - Droplet explosion delay time (*dt*) at different smelt (T_s) and water (T_w) temperatures.

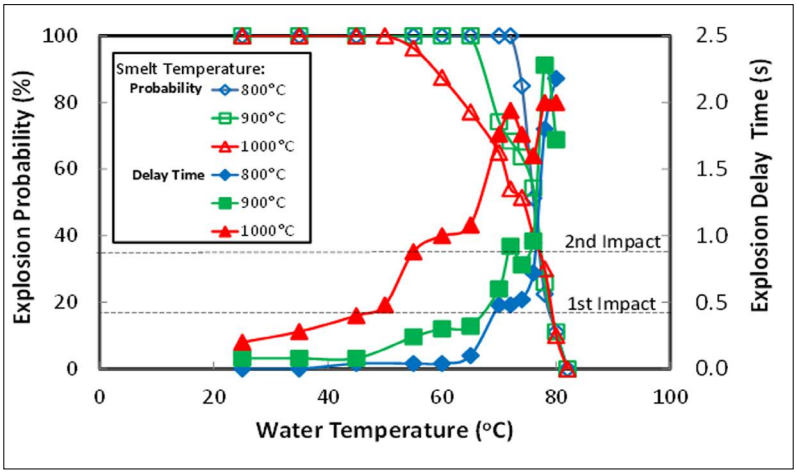

Fig. 14 - Explosion probability (left) and delay time (right) at different smelt and water temperatures.

impact may not explode. The second plateau appears at dt = 0.8 s for T_s =900°C and 1000°C and corresponds to droplets that survived the first impact, bounced up, and impacted the tank bottom a second time. In a sense, the existence of the tank bottom shifts the explosion probability curve upwards. The delay time increases asymptotically towards infinity when the upper $T_{crit,w}$ is reached and the smelt droplets no longer explode. The data become more scattered as the delay time increases, which reflects the stochastic nature of smelt explosions and/or the low probability of explosions at high water temperature.

SUMMARY AND FUTURE WORK

Results have been presented of two complementary studies related to recovery boiler dissolving tank operation. These studies were conducted to understand and improve current practices and will be used as the basis for developing a model of overall dissolving tank operation.

The study of smelt shattering, using air and water as proxies for steam and smelt, clearly demonstrates the effect of shatter-jet nozzle geometry on shattering efficacy. The experimental results indicate that round nozzles produce a more focussed jet that shatters the liquid stream into smaller droplets. Flat nozzles, on the other hand, yield a more dispersed jet that does not shatter as well and tends to displace the liquid stream further from the spout exit.

The study of smelt/water interaction and on the effects of smelt and water temperatures has yielded intriguing results. For the synthetic smelt that was used (80wt% Na_2CO_3 and 20wt% NaCl), smelt droplets interact with water in a number of different ways; this behaviour is a strong function of water temperature. At lower water temperatures, droplets "explode" on contact with the water. With increasing water temperature, smelt droplets are able to penetrate the water surface before exploding, and at some temperature that is a function of the smelt temperature, droplets begin not to explode at all, but rather to solidify on the tank bottom. For the smelt composition studied here, no droplets exploded beyond a water temperature of 82°C, independently of smelt temperature.

These initial studies offer insights into how molten smelt is shattered by a steam jet and how a molten smelt droplet behaves in water. However, many questions must yet be addressed before meaningful conclusions can be drawn. The authors' work on assessing different shatter-jet nozzle profiles will continue in an effort to identify nozzles that shatter better than others, or that shatter as effectively as others while using less air (i.e., steam). Additional experiments will be conducted to look at droplet size distributions on other planes beneath the spout, to predict the spray growth pattern. The intention is to correlate droplet size distributions with appropriate non-dimensional parameters to extrapolate experimental results to predict droplet size distributions at a mill scale. Questions for future research include: How does shatter-jet nozzle placement, relative to the spout, affect shattering? And how well can we expect to shatter so-called "jelly roll smelt" that is very viscous?

The experimental work on smelt/water interaction will also continue. The experimental apparatus is currently being rebuilt to make it possible to vary a number of parameters, including smelt droplet size, smelt composition, green liquor concentration, and the distance that droplets fall before reaching the tank. Acoustic and vibration data will be collected to analyze the intensity of droplet explosions. Questions for future research include: How does the explosion probability vary with smelt droplet size and distribution? Does partially molten smelt explode? Does the distance between the smelt spout and the liquor level in the dissolving tank affect the tendency for immediate explosions? How does one exploding droplet affect the tendency for other droplets to explode? Can we quantify synergetic effects between exploding droplets? How do green liquor composition and concentration affect the tendency for droplets to explode? How can our laboratory-scale results be applied to mill conditions?

ACKNOWLEDGEMENTS

This work was conducted as part of the research program on "Increasing Energy and Chemical Recovery Efficiency in the Kraft Process - III", jointly supported by the Natural Sciences and Engineering Research Council of Canada (NSERC) and a consortium of the following companies: Andritz, AV Nackawic, Babcock & Wilcox, Boise, Carter Holt Harvey, Celulose Nipo-Brasileira, Clyde-Bergemann, DMI Peace River Pulp, Eldorado, ERCO Worldwide, Fibria, FPInnovations, International Paper, Irving Pulp & Paper, Kiln Flame Systems, Klabin, MeadWestvaco, Metso Power, StoraEnso Research, Suzano, Tembec, and Tolko Industries.

REFERENCES

1. Grace, T.M., "Chapter 11 - Recovery Boiler Safety", in Adams, T.N. (Ed.), Kraft Recovery Boilers, TAPPI Press, Atlanta (1997).
2. Lien, S. and DeMartini, N. "Dissolving Tank Explosions: A Review of Incidents between 1973 and 2008". Unpublished report to BLRBAC and AF&PA, sponsored by the American Forest & Paper Association, New York (2008).
3. Shick, P.E. and Grace, T.M. "Review of Smelt-Water Explosions", Proceedings of the International Chemical Recovery Conference, pp. 155-164, Vancouver (1981).
4. Dullforce, T.A., Buchanan, D.J., and Peckover, R.S., "Self-Triggering of Small Scale Fuel-Coolant Interaction: I. Experiments", Journal of Physics D: Applied Physics, 9: 1295-1303 (1976).
5. Buchanan, D.J. and Dullforce, T.A., "Mechanism of Vapor Explosions", Nature, 245, 32-34 (1973).
6. Reid, R.C., "Rapid Phase Transitions from Liquid to Vapour", Advances in Chemical Engineering, 12, 105-208 (1983).
7. Epstein, S.G., "Molten Aluminum-Water Explosions: An Update", In

Das, S.K. (Ed.), Light Metals 1993, Metallurgical Society of AIME, 845-853 (1992).
8. Katz, D.L. and Sliepcevich, C.M., "Liquefied Natural Gas/Water Explosions: Cause and Effect", Hydrocarbon Processing, 50, 240-244 (1971).
9. Corradini, M.L., Kim, B.J., and Oh, M.D., "Vapor Explosions in Light Water Reactors: A Review of Theory and Modeling", Progress in Nuclear Energy, 22(1), 1-117 (1988).
10. Francis, P. and Self, S. "The Eruption of Krakatau", Scientific American, 249, 149-159 (1983).
11. Sallack, J.A., "An Investigation of Explosions in the Soda Smelt Dissolving Operation", Pulp Paper Canada Magazine, 56(10): 114-118 (1955).
12. Nelson, W. and Kennedy, E.H., "What Causes Kraft Dissolving Tank Explosions, I. Laboratory Experiments", Paper Trade Journal, 140(29): 50-56 (1956).
13. Taranenko, A., "Shattering Recovery Boiler Smelt by a Steam Jet", M.A.Sc. thesis, University of Toronto (2012).
14. Taranenko, A., Bussmann, M., and Tran, H.N., "A Laboratory Study of Recovery Boiler Smelt Shattering", Proceedings of TAPPI PEERS, Green Bay, WI (2013).
15. ImageJ, developed at the National Institutes of Health, available at www.imagej.net.
16. Jin, E., "Interaction between a Molten Smelt Droplet and Water", M.A.Sc. thesis, University of Toronto (2013).
17. Jin, E., Bussmann, M., and Tran, H.N., "An Experimental Study of Smelt-Water Interaction in the Recovery Boiler Dissolving Tank", Proceedings of TAPPI PEERS, Green Bay, WI (2013).